

Tight-Binding Bandstructure of β - and α - phase Ga_2O_3 and Al_2O_3

Y. Zhang,^{1, a)} M. Liu,² G. Khalsa,^{2, b)} and D. Jena^{1, 2}¹⁾Electrical and Computer Engineering, Cornell University, Ithaca, NY 14850, USA²⁾Materials Science and Engineering, Cornell University, Ithaca, NY 14850, USA

(Dated: 9 November 2021)

Rapid design and development of the emergent ultra-wide bandgap semiconductors Ga_2O_3 and Al_2O_3 requires a compact model of their electronic structures, accurate over the broad energy range accessed in future high-field, high-frequency, and high-temperature electronics and visible and ultraviolet photonics. A minimal tight-binding model is developed to reproduce the first-principles electronic structures of the β - and α - phases of Ga_2O_3 and Al_2O_3 throughout their reciprocal spaces. Accurately reproducing the bandgap, orbital character, and effective mass and high-energy features of the conduction band, this compact model will assist in the investigation and design of the electrical and optical properties of bulk materials, devices, and quantum confined heterostructures.

I. INTRODUCTION

The recent integration of Ga_2O_3 with Al_2O_3 has the potential to revolutionize high-power electronics. The availability of large, inexpensive, single-crystal substrates^{1, 2}, recent advances in thin film growth³⁻⁵, and the ability to dope these wide-bandgap semiconductors have enabled transistors and Schottky diodes based on β - Ga_2O_3 with breakdown fields as large as 5.45 MV/cm (Ref. 6) and 5.7 MV/cm (Ref. 7) and approaching the projected theoretical estimate of 8 MV/cm (Ref. 8). Comparing these breakdown fields with the existing technological semiconductors Si (0.3 MV/cm), SiC (3.1 MV/cm), and GaN (3.3 MV/cm)⁹, β - Ga_2O_3 promises new high-frequency, high-voltage, and high-temperature electronics applications. α - Ga_2O_3 and α - Al_2O_3 further expand the bandgap to 5.2 eV and 8.8 eV, signifying the potential for oxide semiconductors to expand the future electronics materials tool-set.

The successful design of these future electronic devices requires an accurate modeling and understanding of the electronic structure and bonding of Ga_2O_3 and Al_2O_3 . The tight-binding method provides a flexible, chemically motivated description of the electronic structure of materials¹⁰. When compared with modern computational approaches to materials physics like density functional theory (DFT), tight-binding models are compact, intuitive, and require less computational resources. As a result, tight-binding models are ubiquitous in device engineering and development and have successfully described electronic transport¹¹⁻¹⁵ and optical properties^{14, 16-18} of bulk materials, heterostructures, and devices. To aid in the development of new high-power electronics, we derive semi-empirical tight-binding models in this work for three technologically relevant oxide semiconductors: β - Ga_2O_3 , α - Ga_2O_3 , and α - Al_2O_3 .

While we are unaware of a tight-binding model describing these three oxide semiconductors, a recent study reports a tight-binding model of β - Ga_2O_3 using atomic orbitals as a basis, with parameters drawn from DFT calculations¹⁹. The

authors employ the model to study the surface energy of β - Ga_2O_3 and formation energy of Ga and O vacancy defects. We derive an alternative tight-binding model with the goal of accurate parameterization of the conduction band and fundamental optical gaps of β - Ga_2O_3 , α - Ga_2O_3 and α - Al_2O_3 so that electrical and optical properties can be faithfully simulated.

We derive tight-binding models using a Wannier functions basis. Wannier functions are a convenient basis for tight-binding models because they are derived from the underlying band structure of the material, are formally orthogonal, can be localized to atomic sites, and preserve the site symmetry and coordination. This approach of DFT-derived tight-binding has been used successfully to describe the electronic structure of broad classes of technologically important materials including silicon²⁰, III-V semiconductors²¹, and 2D materials²².

II. STRUCTURAL AND ELECTRICAL PROPERTIES

The crystal symmetry and bonding environment constrain the tight-binding description of the electronic structure. When compared to a conventional semiconductor like Si, Ga_2O_3 and Al_2O_3 have relatively low symmetry and complicated bonding networks. β - Ga_2O_3 has a monoclinic structure (space group C2/m, No. 12). The monoclinic structure contains two pairs of symmetry inequivalent Ga sites, each coordinated by O, forming two distorted GaO_4 tetrahedra and two distorted GaO_6 octahedra per unit cell (Fig. 1(a)). α - Al_2O_3 and α - Ga_2O_3 crystallize in the sapphire structure (rhombohedral, space group R-3c, No. 167). In the α phase, the Al(Ga) atoms occupy 4 equivalent sites, each coordinated by six O, forming distorted $\text{AlO}_6(\text{GaO}_6)$ octahedra (Fig. 1(b)). The structural information obtained from DFT structural optimization and experimental data are given in Table I where DFT is shown to describe the experimental structure surprisingly well. The valence configurations of O, Al, and Ga are $2s^2 2p^4$, $3s^2 3p^1$, and $4s^2 4p^1$, respectively. The Al(Ga) is expected to donate its valence electrons in order to fill the O valence shell, leading to an O-2p derived valence band with Al-3s(Ga-4s) and Al-3p(Ga-4p) derived conduction band.

Structural optimization and electronic band structure are calculated by DFT using Quantum Espresso²³. We

^{a)}Electronic mail: yz2439@cornell.edu.^{b)}Electronic mail: guru.khalsa@cornell.edu.

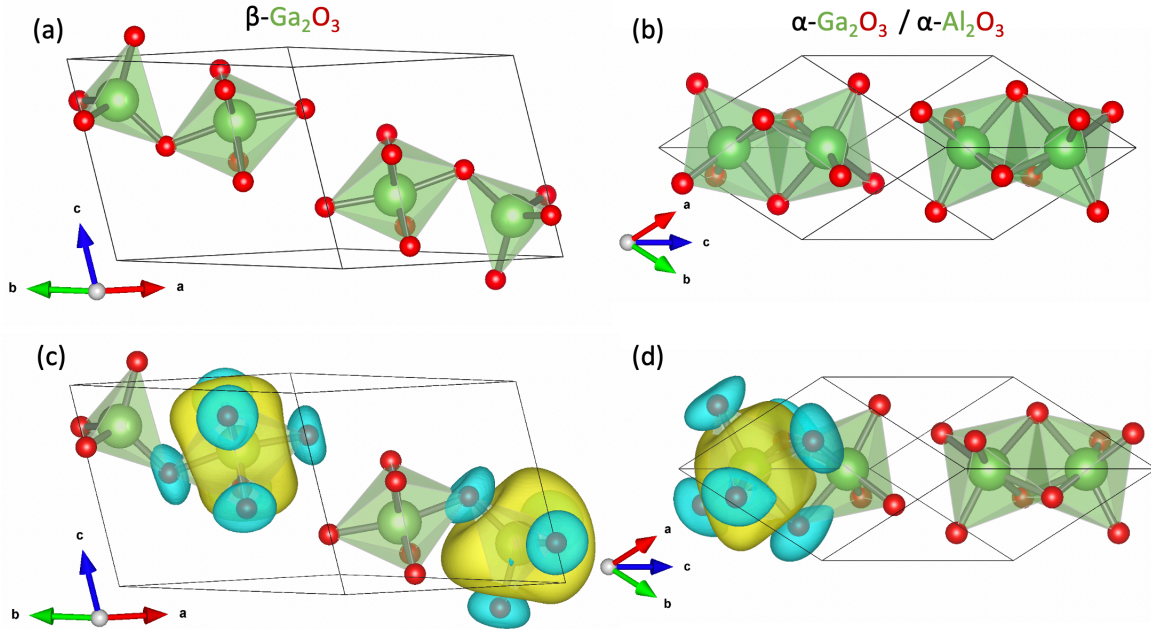


FIG. 1: Crystal structure of monoclinic β - Ga_2O_3 , and rhombohedral α - Ga_2O_3 and α - Al_2O_3 . Coordination octahedra and tetrahedra highlight the different Ga(Al)-O bonding environments in the β (a) and α (b) phases. This bonding difference is evident in the symmetry of Ga(Al)-site Wannier functions (c,d) for the conduction band where clear hybridization of the Ga(Al)-s and O-p is seen. In (c,d), the positive lobes of the Wannier functions are shown in yellow and the negative lobes are shown in blue.

choose projector-augmented wave pseudopotentials and generalized-gradient approximation of exchange correlation using the Perdew-Burke-Ernzerhof functional generalized for solids^{24,25}. Structural convergence is found for a $3 \times 3 \times 3$ k-point mesh and a 60 Ry plane-wave cutoff. We find good agreement between the DFT-relaxed structure and the experimental structure (see Table I).

The DFT band structure and DOS are shown in Fig. 2(c,f,i) and found to be in agreement with previous work²⁹. Orbital projected DOS shows the valence band is primarily O-2p and the conduction band is primarily Ga-4s(Al-3s) and Ga-4p(Al-3p). The bottom of the conduction band is dominated by Ga-4s(Al-3s) states, transitioning to mainly Ga-4p(Al-3p) in character at 6 eV above the conduction band minimum. All three materials share several broad features of their band structure: broad O-2p valence bands with a flat valence band edges, conduction band edge features near the Γ point, and indirect bandgaps. In all three materials, the valence band edge is populated by flat O-2p bands. DFT predicts the valence band maximum between M_2 and D in β - Ga_2O_3 , and between Γ and S_0 in both α - Ga_2O_3 and α - Al_2O_3 . The conduction band minimum at the Γ -point has nearly isotropic dispersion, suggesting that it is insensitive to symmetry and chemistry. We find an effective mass of $0.26 m_e$ in β - Ga_2O_3 , $0.28 m_e$ in α - Ga_2O_3 , and $0.42 m_e$ in α - Al_2O_3 . We found that the conduction band effective mass of β - Ga_2O_3 is in good agreement with recent transport³⁰ and angle-resolved photoemission spectroscopy^{31,32} (ARPES) experiments. Away from the band minimum, the conduction band transitions from

parabolic to linear dispersion, a band structure feature used to explain high field transport^{33,34} and optical absorption³⁵ experiments. The second conduction band at the Γ point is above the conduction band minimum by 3.3 eV in β - Ga_2O_3 , 3.5 eV in α - Ga_2O_3 , and 3.1 eV in α - Al_2O_3 , respectively. The value of β - Ga_2O_3 agrees with the experimental observation of 3.55 eV³⁵. DFT predicts an indirect bandgap with the difference between the direct and indirect bandgap less than 20 meV. This is confirmed by the ARPES measurement^{31,32}. As expected, the bandgap predicted by DFT underestimates the experimental bandgaps. In order to match the experimental bandgap, we have conducted a “scissor cut” by shifting the conduction band states up in energy so that the bandgaps match the experimental values of 4.9 eV³², 5.2 eV³⁶, and 8.8 eV³⁷ in β - Ga_2O_3 , α - Ga_2O_3 , and α - Al_2O_3 , respectively. In constructing a tight-binding model, we aim to describe the above key features of the DFT band structure.

III. TIGHT-BINDING DERIVATION

We derive Wannier functions from the DFT band structure using Wannier90³⁸ to construct the tight-binding basis. Wannier functions are initialized on the Ga(Al) sites with s- and p-orbital symmetry and on the O sites with p-orbital symmetry. We selectively localize only the Ga-s(Al-s) Wannier functions onto Ga(Al) sites using a Lagrange multiplier³⁹. Selectively-localized Wannier functions improve the localization of Ga-s(Al-s) Wannier functions at the cost of delocalizing Ga-p(Al-

TABLE I: β - Ga_2O_3 , α - Ga_2O_3 , and α - Al_2O_3 structural data. In the β -phase (left column), Ga and O occupy the i Wyckoff site with fractional coordinates $(x, 0, z)$ and $(-x, 0, -z)$. In the α phase (right column), Ga(Al) occupy the c Wyckoff site with fractional coordinates (z, z, z) , $(-z + \frac{1}{2}, -z + \frac{1}{2}, -z + \frac{1}{2})$, $(-z, -z, -z)$, and $(z + \frac{1}{2}, z + \frac{1}{2}, z + \frac{1}{2})$ and O occupies the e Wyckoff site with fractional coordinates $(x + \frac{1}{4}, -x + \frac{1}{4}, \frac{1}{4})$, $(\frac{1}{4}, x + \frac{1}{4}, -x + \frac{1}{4})$, $(-x + \frac{1}{4}, \frac{1}{4}, x + \frac{1}{4})$, $(-x + \frac{3}{4}, x + \frac{3}{4}, \frac{3}{4})$, $(\frac{3}{4}, -x + \frac{3}{4}, x + \frac{3}{4})$, and $(x + \frac{3}{4}, \frac{3}{4}, -x + \frac{3}{4})$.

β - Ga_2O_3	a (Å)	b (Å)	c (Å)	β (°)
DFT	12.237	3.062	5.813	103.81
Experiment ²⁶	12.214	3.037	5.798	103.83

β - Ga_2O_3	Ga(I) (4i)		Ga(II) (4i)	
	x	z	x	z
DFT	0.0904	0.7949	0.6585	0.3137
Experiment ²⁶	0.0895	0.7938	0.6585	0.3100

α - Ga_2O_3	a (Å)	b (Å)	Ga(I) 4c	O(I) 6e
DFT	5.3221	55.82	$z=0.1446$	$x=0.3049$
Experiment ²⁷	5.3221	55.82	$z=0.1446$	$x=0.3049$

α - Al_2O_3	a (Å)	b (Å)	Al(I) 4c	O(I) 6e
DFT	5.1779	55.28	$z=0.1479$	$x=0.3056$
Experiment ²⁸	5.126	55.25	$z=0.3522$	$x=0.3064$

β - Ga_2O_3	O(I) (4i)		O(II) (4i)		O(III) (4i)	
	x	z	x	z	x	z
DFT	0.1647	0.1094	0.1733	0.5632	0.4959	0.2563
Experiment ²⁶	0.1519	0.1001	0.1722	0.5640	0.4920	0.2645

p) Wannier functions which describe the higher conduction bands (> 5 eV above the conduction band minimum). We find that the O-p Wannier functions have similar localization in both schemes.

We show isosurface plots of Ga-s Wannier functions in β and α phases resulting from selective localization in Fig. 1(c,d). (The Al-s and Ga-s Wannier functions in the α phase are qualitatively similar.) The Wannier functions reproduce the distorted tetrahedral and octahedral symmetry of the coordination polyhedra as expected from the hybridization between the Ga-4s and O-2p atomic orbitals in Ga_2O_3 .

We construct the tight-binding model from the Wannier function basis by extracting the Hamiltonian matrix element using PythTB⁴⁰. We parameterize our tight-binding model in the following form:

$$\hat{H} = \sum_i \varepsilon_i |i\rangle \langle i| + \sum_{i,j} t_{ij} e^{-i\vec{k} \cdot \Delta \vec{d}_{ij}} |j\rangle \langle i| + c.c. \quad (1)$$

The right-hand side of the first line describes the contribution of individual Wannier functions to the total energy, commonly called the onsite energy. The second line describes the kinetic energy of the electrons, commonly called the ‘‘hopping’’ energy. In Equation (1), $|i\rangle$ represents the i^{th} Wannier function with on-site energy ε_i . $t_{ij} = \tilde{t}_{ij} e^{i\phi_{ij}}$ is the hopping term between i^{th} and j^{th} Wannier functions. Here ϕ_{ij} characterizes the phase of t_{ij} and encompasses the symmetry of the local bonding environment. \vec{k} is the wavevector, and $\Delta \vec{d}_{ij}$ is the displacement vector of the two Wannier functions i and j defined as $\Delta \vec{d}_{ij} = \vec{d}_j - \vec{d}_i + \vec{R}$. Here \vec{d}_i and \vec{d}_j are the centers of Wannier function i and j within the same unit cell, and \vec{R} is the unit cell translation to indicate coupling across adjacent unit cells.

In our tight-binding model, we include only the s-orbital-derived Wannier functions from the 4 Ga(Al) atoms and the 3 p-orbital-derived Wannier functions from the 6 O atoms. This

translates to a 22×22 matrix when the model is implemented numerically. To describe the band structure with a minimal set of parameters, we include: 1) the onsite energy (ε_i terms for Ga-s(Al-s) and O-p, 2) the nearest-neighbor Ga-s(Al-s) to O-p and, 3) the dominant Ga-s(Al-s) to Ga-s(Al-s) terms (t_{ij}). This amounts to a nearest-neighbor tight-binding model augmented by the Ga-s(Al-s) to Ga-s(Al-s) next-nearest-neighbor hopping. These next-nearest-neighbor terms aid in the accuracy of the higher Ga-4s(Al-3s) derived conduction bands. With these simplifications, the model contains 60 parameters depending on the structural phases (see Table SIII to SV). Including the Ga-p(Al-p) Wannier functions and O-p to O-p coupling terms gives a satisfactory description of valence band DOS at the cost of significantly increasing the number of parameters (around 300 terms), but provides little improvement to the description of the lower conduction bands. Thus, we neglect these terms in our model.

To reproduce the experimental bandgaps and conduction band effective masses, we adjust the Ga-s(Al-s) onsite energy and tune the Ga-s(Al-s) to O-p coupling term. (We note that in their model of β - Ga_2O_3 , Lee, et al.¹⁹ focus on surface and defect formation energies which depend on the broad features of the band structure. As a result, their tight-binding model overestimates the conduction band effective mass.) The lists of parameters are given in Table SIII, SIV, and SV.

When implementing the tight-binding model on a computer, Eq. (1) can be written as a 22×22 matrix defined over the basis of 4 Ga-s(Al-s) and 18 O-p Wannier functions. In evaluating the model, the on-site energy ε_i become diagonal terms while the hopping terms t_{ij} populate the i^{th} row and j^{th} column and must be multiplied by the phase factor $e^{-i\vec{k} \cdot \Delta \vec{d}_{ij}}$ at each k-point. To illustrate the model and gain insight into the material physics, we explicitly evaluate the tight-binding model of β - Ga_2O_3 at the Γ -point ($\vec{k} = \vec{0}$). We find that the tight-binding model at the Γ -point can be written in the block-matrix form:

$$H = \begin{pmatrix} H_{\text{Ga}:s} & H_{\text{Ga}:s,\text{O}:p_x}^\dagger & 0 & H_{\text{Ga}:s,\text{O}:p_z}^\dagger \\ H_{\text{Ga}:s,\text{O}:p_x} & H_{\text{O}:p_x} & 0 & 0 \\ 0 & 0 & H_{\text{O}:p_y} & 0 \\ H_{\text{Ga}:s,\text{O}:p_z} & 0 & 0 & H_{\text{O}:p_z} \end{pmatrix} \quad (2)$$

where the $H_{\text{Ga}:s}$, $H_{\text{O}:p_x}$, $H_{\text{O}:p_y}$, and $H_{\text{O}:p_z}$ blocks define the coupling within the Ga-s, O- p_x , O- p_y , and O- p_z Wannier function sub-spaces, respectively. The $H_{\text{Ga}:s,\text{O}:p_x}$ and $H_{\text{Ga}:s,\text{O}:p_z}$ blocks describe the coupling between the Ga-s and O- p_x , and O- p_z Wannier functions, respectively. We construct the tight-

$$H_{\text{Ga}:s} = \begin{pmatrix} \epsilon_{\text{Ga}1:s} + 2t_{\text{Ga}1:s,\text{Ga}1:s} & 0 & 0 & 0 \\ 0 & \epsilon_{\text{Ga}1:s} + 2t_{\text{Ga}1:s,\text{Ga}1:s} & 0 & 0 \\ 0 & 0 & \epsilon_{\text{Ga}3:s} + 2t_{\text{Ga}3:s,\text{Ga}3:s} & t_{\text{Ga}3:s,\text{Ga}4:s} \\ 0 & 0 & t_{\text{Ga}3:s,\text{Ga}4:s} & \epsilon_{\text{Ga}3:s} + 2t_{\text{Ga}3:s,\text{Ga}3:s} \end{pmatrix} \quad (3)$$

$$\rightarrow \begin{pmatrix} -7.498 & 0 & 0 & 0 \\ 0 & -7.498 & 0 & 0 \\ 0 & 0 & -7.222 & 0.216 \\ 0 & 0 & 0.216 & -7.222 \end{pmatrix}$$

which is written in the basis ($|\text{Ga}1:s\rangle, |\text{Ga}2:s\rangle, |\text{Ga}3:s\rangle, |\text{Ga}4:s\rangle$) of Ga-s Wannier functions. Taking values from Table SIII, we have included the numerical value of the block in eV. Since Ga1:s and Ga2:s are equivalent tetrahedral sites while Ga3:s and Ga4:s are equivalent octahedral sites, each have the same onsite energy and coupling. Notice that the onsite energy $\epsilon_{\text{Ga}1:s}$ and $\epsilon_{\text{Ga}3:s}$ are modified by coupling to the same Ga sites in the neighboring unit cells ($t_{\text{Ga}1:s,\text{Ga}1:s}$ and $t_{\text{Ga}3:s,\text{Ga}3:s}$). Furthermore, the octahedral sites are weakly coupled to each other.

In simplifying the description of the valence band, we neglect the coupling between O- p Wannier functions. As a result each $H_{\text{O}:p_x}$, $H_{\text{O}:p_y}$, and $H_{\text{O}:p_z}$ block is diagonal and can be

binding model so that it reflects the crystal symmetry. This can be seen clearly in the lack of coupling between the Ga-s and O- p_y Wannier functions. The two-fold rotation about the crystallographic b-axis and the mirror operation through the plane perpendicular to the b-axis guarantee this coupling is zero at the Γ -point. The coupling between different O- p Wannier function blocks (e.g. O- p_x and O- p_y) are zero because we have neglected the coupling within the valence band. At the Γ point, the phase factor $e^{-i\vec{k}\cdot\Delta\vec{d}_{ij}} \rightarrow 1$, leaving the matrix real and symmetric.

$H_{\text{Ga}:s}$ takes the form:

written as:

$$H_{\text{O}:p_x} = H_{\text{O}:p_y} = H_{\text{O}:p_z} = \epsilon_{\text{O}:p} \times \mathbb{I}_{6\times 6} \rightarrow -12 \times \mathbb{I}_{6\times 6} \quad (4)$$

which is written in the basis ($|\text{O}1:p_l\rangle, |\text{O}2:p_l\rangle, |\text{O}3:p_l\rangle, |\text{O}4:p_l\rangle, |\text{O}5:p_l\rangle, |\text{O}6:p_l\rangle$), of O- p Wannier functions where $l = x, y, z$. Here, $\mathbb{I}_{6\times 6}$ is the 6×6 identity matrix.

The coupling between Ga-s and O- p_x and O- p_z are described by $H_{\text{Ga}:s,\text{O}:p_x}$ and $H_{\text{Ga}:s,\text{O}:p_z}$ which evaluate to (hopping strengths connected by symmetries are shown with the same symbol):

$$H_{\text{Ga}:s,\text{O}:p_x} = \begin{pmatrix} t_{\text{Ga}1:s,\text{O}1:p_x} & 0 & 2t_{\text{Ga}3:s,\text{O}1:p_x} & 0 \\ 0 & -t_{\text{Ga}1:s,\text{O}1:p_x} & 0 & 2t_{\text{Ga}4:s,\text{O}2:p_x} \\ t_{\text{Ga}1:s,\text{O}3:p_x} & 0 & 0 & -t_{\text{Ga}3:s,\text{O}4:p_x} \\ 0 & t_{\text{Ga}2:s,\text{O}4:p_x} & t_{\text{Ga}3:s,\text{O}4:p_x} & 0 \\ 0 & -2t_{\text{Ga}1:s,\text{O}6:p_x} & t_{\text{Ga}3:s,\text{O}5:p_x} & 0 \\ 2t_{\text{Ga}1:s,\text{O}6:p_x} & 0 & 0 & -t_{\text{Ga}3:s,\text{O}5:p_x} \end{pmatrix} \rightarrow \begin{pmatrix} 0.651 & 0 & 0.710 & 0 \\ 0 & -0.651 & 0 & -0.703 \\ 2.592 & 0 & 0 & -2.877 \\ 0 & -2.595 & 2.877 & 0 \\ 0 & 3.499 & -2.965 & 0 \\ -3.496 & 0 & 0 & 2.965 \end{pmatrix} \quad (5)$$

$$H_{\text{Ga}:s,\text{O}:p_z} = \begin{pmatrix} t_{\text{Ga}1:s,\text{O}1:p_z} & 0 & 2t_{\text{Ga}3:s,\text{O}1:p_z} & 0 \\ 0 & -t_{\text{Ga}1:s,\text{O}1:p_z} & 0 & 2t_{\text{Ga}4:s,\text{O}2:p_z} \\ t_{\text{Ga}1:s,\text{O}3:p_z} & 0 & 2t_{\text{Ga}3:s,\text{O}3:p_z} & -t_{\text{Ga}3:s,\text{O}4:p_z} \\ 0 & -t_{\text{Ga}2:s,\text{O}4:p_z} & t_{\text{Ga}3:s,\text{O}4:p_z} & -2t_{\text{Ga}4:s,\text{O}4:p_z} \\ 0 & -2t_{\text{Ga}1:s,\text{O}6:p_z} & t_{\text{Ga}3:s,\text{O}5:p_z} & 0 \\ 2t_{\text{Ga}1:s,\text{O}6:p_z} & 0 & 0 & -t_{\text{Ga}3:s,\text{O}5:p_z} \end{pmatrix} \rightarrow \begin{pmatrix} 3.466 & 0 & -3.307 & 0 \\ 0 & -3.466 & 0 & 3.314 \\ 2.592 & 0 & 3.345 & -1.101 \\ 0 & 2.595 & 1.101 & -3.326 \\ 0 & 0.885 & -0.621 & 0 \\ -0.880 & 0 & 0 & 0.621 \end{pmatrix} \quad (6)$$

Here, terms appear as pairs with opposite signs, manifesting

the two-fold symmetry of the monoclinic structure. $H_{\text{Ga}:s,\text{O}:p_x}$

and $H_{\text{Ga}s,\text{O}:pz}$ looks formally similar but are not exactly the same. Again, the matrix coupling Ga-s to O-py vanishes at the Γ point but will show up away from it. The complete set of matrix elements can be found in Table SIII. The eigenvalues of the 22×22 matrix correspond to the energy eigenstates at the given k-point, and the eigenvectors correspond to the wavefunctions. To generate the band structure, one generates the matrix at sampled k-points along the path and solve for the eigenvalues. The complexity of numerical eigensolvers depends on the matrix dimension as $O(n^3)$. As a comparison, our DFT calculation relies on around 5000 planar waves as a basis, so the tight-binding model provides a significant speedup. In our experience, a tight-binding band structure can be generated on a personal computer in seconds.

IV. TIGHT-BINDING BANDSTRUCTURE

Fig. 2(d,g,j) shows the tight-binding band structure and DOS superimposed on the DFT results. In all three phases, the experimental bandgaps and conduction band effective masses are reproduced by the adjustment of parameters mentioned above. Moreover, the tight-binding model gives a satisfactory description of the parabolic to linear dispersion, the second conduction band at the Γ point, and the flat valence band edge states.

The slope of the linear dispersion of the lowest conduction band away from Γ , and the energy of the second conduction band at Γ are slightly overestimated due to the absence of interaction from higher Ga-p(Al-p) bands. This phenomenon is well-known in the tight-binding description of Si, Ge, and III-V semiconductors⁴¹ where it is due to the lack of interactions from higher energy bands. The lack of O-p to O-p coupling leaves some of the O-p states non-dispersive. As a result, the tight-binding model cannot describe the small difference between the valence band at Γ and the DFT predicted valence band maximum between Γ and T in the β phase and Γ and S_0 in the α phases. This leaves a large peak in the DOS at the valence band edge (see Fig. 2(d-f)) which could be resolved in future models that include O-p to O-p coupling.

V. CONCLUSION

We have derived a minimal tight-binding model for β - Ga_2O_3 , α - Ga_2O_3 , and α - Al_2O_3 using selectively-localized Wannier functions as a basis. The Wannier functions reflect the local symmetry of the atomic sites and the tight-binding model satisfactorily reproduces the electronic structure throughout the Brillouin zone. By constraining the hopping parameters, we have fit the isotropic conduction band effective mass, suggesting low field transport experiments can be described by the tight-binding model. By including the higher energy Ga-s(Al-s) conduction bands, the tight-binding model can also describe the parabolic to linear dispersion which suggests application to high-field electronic transport as well. Finally, by reproducing the experimental bandgap, we expect that the tight-binding model can simulate the ma-

ior features in optical absorption including the primary optical transition from the O-p valence bands to the Ga-s(Al-s) conduction bands, and the optical transition from the valence band to the higher energy conduction bands. We expect the tight-binding models to aid in the description and development of electronic and optical devices utilizing bulk, nanostructured, heterostructured, and strained variants of β - Ga_2O_3 , α - Ga_2O_3 , and α - Al_2O_3 .

ACKNOWLEDGMENTS

This research project was conducted using computational resources at the Maryland Advanced Research Computing Center (MARCC) and was supported by the National Science Foundation (Platform for the Accelerated Realization, Analysis and Discovery of Interface Materials (PARADIM)) under Cooperative Agreement No. DMR-1539918.

DATA AVAILABILITY STATEMENT

The data that supports the findings of this study are available within the article and its supplementary material.

- ¹M. Higashiwaki, K. Sasaki, A. Kuramata, T. Masui, and S. Yamakoshi, "Gallium oxide (Ga_2O_3) metal-semiconductor field-effect transistors on single-crystal β - Ga_2O_3 (010) substrates," *Applied Physics Letters* **100**, 013504 (2012).
- ²A. Kuramata, K. Koshi, S. Watanabe, Y. Yamaoka, T. Masui, and S. Yamakoshi, "High-quality β - Ga_2O_3 single crystals grown by edge-defined film-fed growth," *Japanese Journal of Applied Physics* **55**, 1202A2 (2016).
- ³D. Gogova, G. Wagner, M. Baldini, M. Schmidbauer, K. Irmscher, R. Schewski, Z. Galazka, M. Albrecht, and R. Fornari, "Structural properties of Si-doped β - Ga_2O_3 layers grown by MOVPE," *Journal of Crystal Growth* **401**, 665–669 (2014).
- ⁴H. Okumura, M. Kita, K. Sasaki, A. Kuramata, M. Higashiwaki, and J. S. Speck, "Systematic investigation of the growth rate of β - Ga_2O_3 (010) by plasma-assisted molecular beam epitaxy," *Applied Physics Express* **7**, 095501 (2014).
- ⁵R. Jinno, C. S. Chang, T. Onuma, Y. Cho, S. T. Ho, D. Rowe, M. C. Cao, K. Lee, V. Protasenko, D. G. Schlom, D. A. Muller, H. G. Xing, and D. Jena, "Crystal orientation dictated epitaxy of ultrawide-bandgap 5.4- to 8.6-eV c-(AlGa)2O3 on m-plane sapphire," *Science Advances* **7**, 1–8 (2021), arXiv:2007.03415.
- ⁶S. Roy, A. Bhattacharyya, P. Ranga, H. Splawn, J. Leach, and S. Krishnamoorthy, "High-k Oxide Field-Plated Vertical (001) β - Ga_2O_3 Schottky Barrier Diode with Baliga's Figure of Merit Over 1 GW/cm²," *IEEE Electron Device Letters* **3106**, 1–1 (2021).
- ⁷N. K. Kalarickal, Z. Xia, H.-I. Huang, W. Moore, Y. Liu, M. Brenner, J. Hwang, and S. Rajan, " β -(Al_{0.18}Ga_{0.82})₂O₃ / Ga_2O_3 Double Heterojunction Transistor With Average Field of 5.5 MV/cm," *IEEE Electron Device Letters* **42**, 899–902 (2021).
- ⁸S. J. Pearton, J. Yang, P. H. Cary, F. Ren, J. Kim, M. J. Tadjer, and M. A. Mastro, "A review of Ga₂O₃ materials, processing, and devices," *Applied Physics Reviews* **5**, 011301 (2018).
- ⁹M. Meneghini, G. Meneghesso, and E. Zanoni, *Power GaN Devices: Materials, Applications and Reliability* (Springer International Publishing, 2017).
- ¹⁰W. A. Harrison, *Electronic Structure and the Properties of Solids - The Physics of the Chemical Bond* (Dover Publications, 1989).
- ¹¹S. Datta, *Quantum Transport: Atom to Transistor* (Cambridge University Press, 2005).

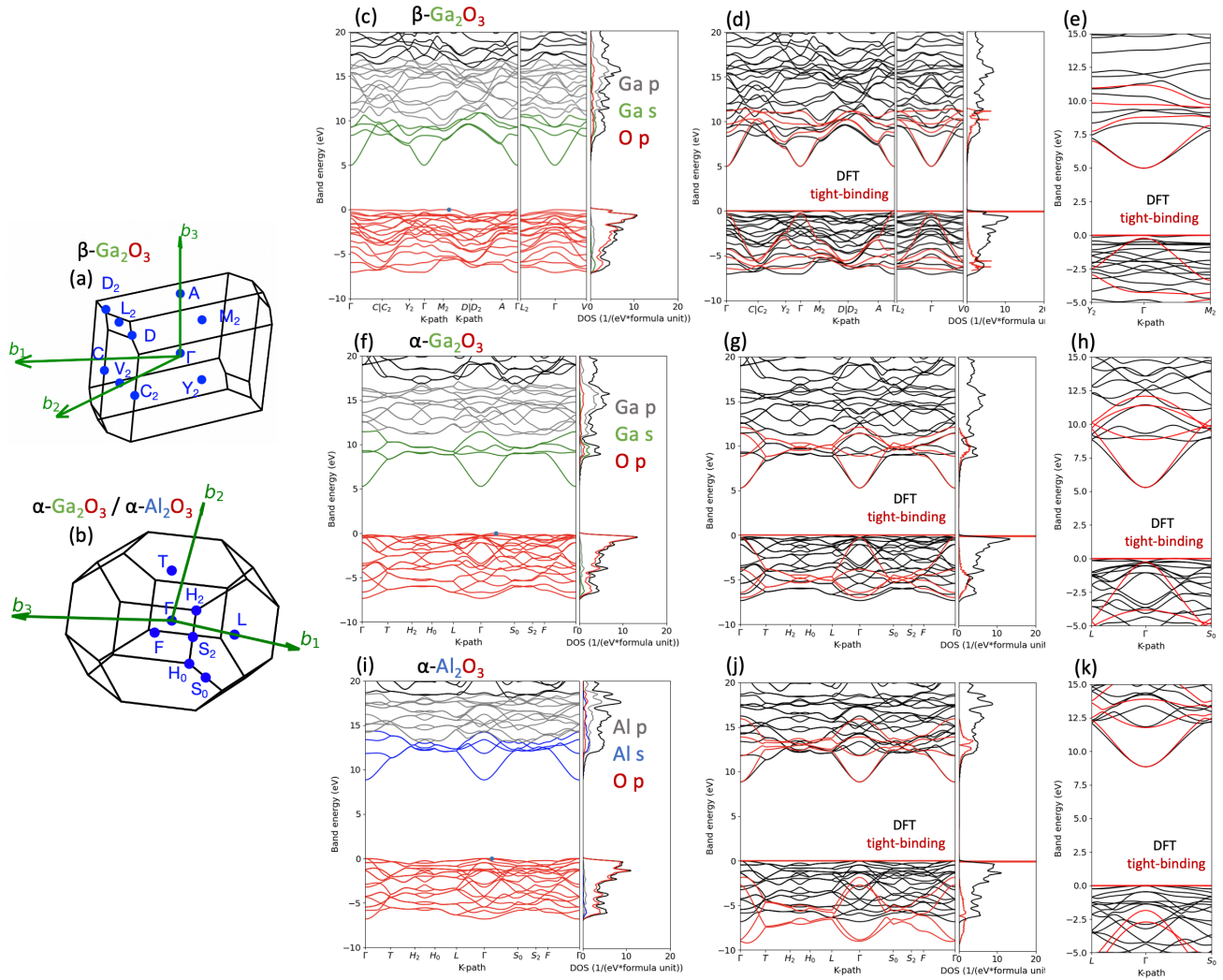


FIG. 2: Electronic structure of β - Ga_2O_3 , α - Ga_2O_3 , and α - Al_2O_3 . (a,b) – The first Brillouin zone of the monoclinic β and rhombohedral α phases. (c,f,i) – The DFT band structure and orbital-projected DOS of β - Ga_2O_3 , α - Ga_2O_3 , and α - Al_2O_3 . The DFT bandgaps have been tuned to the experimental bandgaps via a scissor cut. Color coordination indicates the orbital character of the bands and projected DOS. The blue dots indicate the valence band maximum. (d,g,j) – The tight-binding band structure and DOS (red) plotted over the DFT data (black). The sharp peak in the tight-binding DOS at the top of the valence band is due to the lack of O-p to O-p coupling in the tight-binding model. (e,h,k) – DFT (black) and tight-binding (red) band structure near the Γ point. The reciprocal space vectors and high-symmetry points are given in Table SII.

¹²R. Lake, G. Klimeck, R. C. Bowen, and D. Jovanovic, “Single and multi-band modeling of quantum electron transport through layered semiconductor devices,” *Journal of Applied Physics* **81**, 7845–7869 (1997).

¹³K. Nehari, N. Cavassilas, J. L. Autran, M. Bescond, D. Munteanu, and M. Lannoo, “Influence of band-structure on electron ballistic transport in silicon nanowire MOSFETs: An atomistic study,” *Proceedings of ESSDERC 2005: 35th European Solid-State Device Research Conference* **2005**, 229–232 (2005).

¹⁴V. N. Popov, “Curvature effects on the structural, electronic and optical properties of isolated single-walled carbon nanotubes within a symmetry-adapted non-orthogonal tight-binding model,” *New Journal of Physics* **6** (2004), 10.1088/1367-2630/6/1/017.

¹⁵F. Sols, M. MacUcci, U. Ravaioli, and K. Hess, “Theory for a quantum modulated transistor,” *Journal of Applied Physics* **66**, 3892–3906 (1989).

¹⁶M. Graf and P. Vogl, “Electromagnetic fields and dielectric response in empirical tight-binding theory,” *Physical Review B* **51**, 4940–4949 (1995).

¹⁷X. Pi and C. Delerue, “Tight-binding calculations of the optical response of optimally p-doped Si nanocrystals: A model for localized surface plasmon resonance,” *Physical Review Letters* **111**, 1–5 (2013).

¹⁸C. Jirascsek and T. Kubis, “Modeling techniques for quantum cascade lasers,” *Applied Physics Reviews* **1** (2014), 10.1063/1.4863665, arXiv:1412.3563.

¹⁹J. Lee, S. Ganguli, A. K. Roy, and S. C. Badescu, “Density functional tight binding study of β - Ga_2O_3 : Electronic structure, surface energy, and native point defects,” *The Journal of Chemical Physics* **150**, 174706 (2019).

²⁰I. Souza, N. Marzari, and D. Vanderbilt, “Maximally localized Wannier functions for entangled energy bands,” *Physical Review B - Condensed Matter and Materials Physics* **65**, 1–13 (2002), arXiv:0108084 [cond-mat].

²¹D. Gresch, Q. Wu, G. W. Winkler, R. Häuselmann, M. Troyer, and A. A. Soluyanov, “Automated construction of symmetrized Wannier-like tight-binding models from ab initio calculations,” *Physical Review Materials* **2**, 1–15 (2018), arXiv:1805.12148.

- ²²I. Souza, N. Marzari, D. Vanderbilt, M. Higashiwaki, K. Sasaki, A. Karamata, T. Masui, S. Yamakoshi, J. Jung, A. H. Macdonald, H. Peelaers, C. G. Van de Walle, D. Gresch, Q. Wu, G. W. Winkler, R. Häuselmann, M. Troyer, A. A. Soluyanov, C. Franchini, R. Kováčik, M. Marsman, S. Sathyanarayana Murthy, J. He, C. Ederer, G. Kresse, S. Fang, R. Kuate Defo, S. N. Shirodkar, S. Lieu, G. A. Tritsarlis, E. Kaxiras, S. Carr, S. Fang, H. C. Po, A. Vishwanath, and E. Kaxiras, "Ab initio tight-binding Hamiltonian for transition metal dichalcogenides," *Physical Review B - Condensed Matter and Materials Physics* **1**, 1–15 (2012), arXiv:1907.06282.
- ²³P. Giannozzi, S. Baroni, N. Bonini, M. Calandra, R. Car, C. Cavazzoni, D. Ceresoli, G. L. Chiarotti, M. Cococcioni, I. Dabo, A. Dal Corso, S. de Gironcoli, S. Fabris, G. Fratesi, R. Gebauer, U. Gerstmann, C. Gougoussis, A. Kokalj, M. Lazzeri, L. Martin-Samos, N. Marzari, F. Mauri, R. Mazzarello, S. Paolini, A. Pasquarello, L. Paulatto, C. Sbraccia, S. Scandolo, G. Sclauzero, A. P. Seitsonen, A. Smogunov, P. Umari, and R. M. Wentzcovitch, "QUANTUM ESPRESSO: a modular and open-source software project for quantum simulations of materials," *Journal of Physics: Condensed Matter* **21**, 395502 (2009).
- ²⁴J. P. Perdew, K. Burke, and M. Ernzerhof, "Generalized gradient approximation made simple," *Physical Review Letters* **77**, 3865–3868 (1996).
- ²⁵J. P. Perdew, A. Ruzsinszky, G. I. Csonka, O. A. Vydrov, G. E. Scuseria, L. A. Constantin, X. Zhou, and K. Burke, "Restoring the density-gradient expansion for exchange in solids and surfaces," *Physical Review Letters* **100**, 1–4 (2008), arXiv:0711.0156.
- ²⁶V. Zade, B. Malleshm, S. Shantha-Kumar, A. Bronson, and C. V. Ravana, "Interplay between Solubility Limit, Structure, and Optical Properties of Tungsten-Doped Ga 2 O 3 Compounds Synthesized by a Two-Step Calcination Process," *Inorganic Chemistry* **58**, 3707–3716 (2019).
- ²⁷M. Marezio and J. P. Remeika, "Bond Lengths in the α - Ga_2O_3 Structure and the High-Pressure Phase of $\text{Ga}_{2-x}\text{Fe}_x\text{O}_3$," *The Journal of Chemical Physics* **46**, 1862–1865 (1967).
- ²⁸N. Ishizawa, T. Miyata, I. Minato, F. Marumo, and S. Iwai, "A structural investigation of α -Al 2 O 3 at 2170 K," *Acta Crystallographica Section B Structural Crystallography and Crystal Chemistry* **36**, 228–230 (1980).
- ²⁹H. Peelaers and C. G. Van de Walle, "Brillouin zone and band structure of β -Ga 2 O 3," *physica status solidi (b)* **252**, 828–832 (2015).
- ³⁰Y. Zhang, A. Neal, Z. Xia, C. Joishi, J. M. Johnson, Y. Zheng, S. Bajaj, M. Brenner, D. Dorsey, K. Chabak, G. Jessen, J. Hwang, S. Mou, J. P. Heremans, and S. Rajan, "Demonstration of high mobility and quantum transport in modulation-doped β -($\text{Al}_x\text{Ga}_{1-x}$) $_2\text{O}_3/\text{Ga}_2\text{O}_3$ heterostructures," *Applied Physics Letters* **112**, 1–6 (2018).
- ³¹M. Mohamed, C. Janowitz, I. Unger, R. Manzke, Z. Galazka, R. Uecker, R. Fornari, J. R. Weber, J. B. Varley, and C. G. Van De Walle, "The electronic structure of β - Ga_2O_3 ," *Applied Physics Letters* **97** (2010), 10.1063/1.3521255.
- ³²C. Janowitz, V. Scherer, M. Mohamed, A. Krapf, H. Dwell, R. Manzke, Z. Galazka, R. Uecker, K. Irmscher, R. Fornari, M. Michling, D. Schmeißer, J. R. Weber, J. B. Varley, and C. G. Van De Walle, "Experimental electronic structure of In_2O_3 and Ga_2O_3 ," *New Journal of Physics* **13** (2011), 10.1088/1367-2630/13/8/085014.
- ³³K. Ghosh and U. Singiseti, "Ab initio velocity-field curves in monoclinic β - Ga_2O_3 ," *Journal of Applied Physics* **122** (2017), 10.1063/1.4986174.
- ³⁴K. Ghosh and U. Singiseti, "Impact ionization in β - Ga_2O_3 ," *Journal of Applied Physics* **124** (2018), 10.1063/1.5034120.
- ³⁵A. Singh, O. Koksall, N. Tanen, J. McCandless, D. Jena, H. G. Xing, H. Peelaers, and F. Rana, "Intra- and inter-conduction band optical absorption processes in β - Ga_2O_3 ," *Applied Physics Letters* **117**, 072103 (2020), arXiv:2006.14850.
- ³⁶D. Shinohara and S. Fujita, "Heteroepitaxy of corundum-structured α - Ga_2O_3 thin films on α - Ga_2O_3 substrates by ultrasonic mist chemical vapor deposition," *Japanese Journal of Applied Physics* **47**, 7311–7313 (2008).
- ³⁷R. H. French, "Electronic Band Structure of Al_2O_3 , with Comparison to Alon and AlN," *Journal of the American Ceramic Society* **73**, 477–489 (1990).
- ³⁸G. Pizzi, V. Vitale, R. Arita, S. Blügel, F. Freimuth, G. Géranton, M. Gibertini, D. Gresch, C. Johnson, T. Koretsune, J. Ibañez-Azpiroz, H. Lee, J.-M. Lihm, D. Marchand, A. Marrazzo, Y. Mokrousov, J. I. Mustafa, Y. Nohara, Y. Nomura, L. Paulatto, S. Poncé, T. Ponweiser, J. Qiao, F. Thöle, S. S. Tsirkin, M. Wierzbowska, N. Marzari, D. Vanderbilt, I. Souza, A. A. Mostofi, and J. R. Yates, "Wannier90 as a community code: new features and applications," *Journal of Physics: Condensed Matter* **32**, 165902 (2020).
- ³⁹R. Wang, E. A. Lazar, H. Park, A. J. Millis, and C. A. Marianetti, "Selectively localized Wannier functions," *Physical Review B - Condensed Matter and Materials Physics* **90** (2014), 10.1103/PhysRevB.90.165125, arXiv:1407.5124.
- ⁴⁰S. Coh and D. Vanderbilt, "Python tight binding (PythTB)," (2013).
- ⁴¹P. Vogl, H. P. Hjalmarson, and J. D. Dow, "A Semi-empirical tight-binding theory of the electronic structure of semiconductors†," *Journal of Physics and Chemistry of Solids* **44**, 365–378 (1983).
- ⁴²J. Y. Tsao, S. Chowdhury, M. A. Hollis, D. Jena, N. M. Johnson, K. A. Jones, R. J. Kaplar, S. Rajan, C. G. Van de Walle, E. Bellotti, C. L. Chua, R. Collazo, M. E. Coltrin, J. A. Cooper, K. R. Evans, S. Graham, T. A. Grotjohn, E. R. Heller, M. Higashiwaki, M. S. Islam, P. W. Juodawlkis, M. A. Khan, A. D. Koehler, J. H. Leach, U. K. Mishra, R. J. Nemanich, R. C. Pilawa-Podgurski, J. B. Shealy, Z. Sitar, M. J. Tadjer, A. F. Witulski, M. Wraback, and J. A. Simmons, "Ultrawide-Bandgap Semiconductors: Research Opportunities and Challenges," *Advanced Electronic Materials* **4** (2018), 10.1002/aem.201600501.
- ⁴³M. J. Montgomery, T. N. Todorov, and T. N. Todorov, "Tight-binding simulation of current-carrying nanostructures," (2002).
- ⁴⁴A. Paskaleva, D. Spassov, and P. Terziyska, "Electric, dielectric and optical properties of Ga_2O_3 grown by metal organic chemical vapour deposition," *Journal of Physics: Conference Series* **794**, 012017 (2017).
- ⁴⁵J. G. Ruch and G. S. Kino, "Transport Properties of GaAs," *Physical Review* **174**, 921–931 (1968).

Supplemental Information for Tight-Binding Bandstructure of β - and α - phase Ga_2O_3 and Al_2O_3 Y. Zhang¹ M. Liu² D. Jena^{1,2} and G. Khalsa²

1. Department of Electrical and Computer Engineering and 2. Department of Materials Science and Engineering, Cornell University, Ithaca NY 14853, USA

In the Supplementary Tables we include additional information for the tight-binding models of the monoclinic β - Ga_2O_3 , and the rhombohedral α - Ga_2O_3 and α - Al_2O_3 phases. Table SI gives the structural information from density functional theory in scaled coordinates. Table SII shows the high-symmetry points in reciprocal space for the monoclinic and rhombohedral structures. Table SIII-SV give the explicit tight-binding models for each phase.

TABLE SI: Structural parameters of β - Ga_2O_3 , α - Ga_2O_3 , and α - Al_2O_3 . The Cartesian coordinate of a site i is given by $\vec{a}_i = A_1\vec{a}_1 + A_2\vec{a}_2 + A_3\vec{a}_3$

β - Ga_2O_3				α - Ga_2O_3				α - Al_2O_3			
lattice vector (\AA)	x	y	z	lattice vector (\AA)	x	y	z	lattice vector (\AA)	x	y	z
\vec{a}_1	6.115	1.620	0.000	\vec{a}_1	2.491	1.438	4.478	\vec{a}_1	2.403	1.387	4.372
\vec{a}_2	-6.115	1.620	0.000	\vec{a}_2	-2.491	1.438	4.478	\vec{a}_2	-2.403	1.387	4.372
\vec{a}_3	-1.374	0.000	5.635	\vec{a}_3	0.000	-2.877	4.478	\vec{a}_3	0.000	-2.774	44.372
site coordinate	A_1	A_2	A_3	site coordinate	A_1	A_2	A_3	site coordinate	A_1	A_2	A_3
Ga1	0.090	-0.090	0.795	Ga1	0.179	0.179	0.179	Al1	0.818	-0.162	-0.177
Ga2	0.910	0.090	0.205	Ga2	0.678	0.678	-0.322	Al2	0.671	0.659	-0.311
Ga3	0.659	0.341	0.314	Ga3	0.821	-0.179	-0.179	Al3	0.330	0.318	-0.664
Ga4	0.341	-0.341	0.686	Ga4	0.322	0.322	-0.678	Al4	0.174	0.182	0.164
O1	0.165	-0.165	0.109	O1	0.553	-0.053	0.250	O1	0.750	-0.558	0.057
O2	0.835	0.165	0.891	O2	0.941	0.250	-0.441	O2	0.942	0.250	-0.442
O3	0.173	-0.173	0.563	O3	0.250	0.559	-0.059	O3	1.058	-0.250	-0.558
O4	0.827	0.173	0.437	O4	1.059	-0.250	-0.559	O4	0.442	0.058	-0.250
O5	0.496	-0.496	0.256	O5	0.750	-0.559	0.059	O5	0.558	-0.058	0.250
O6	0.504	0.496	0.743	O6	0.441	0.059	-0.250	O6	0.250	0.558	-0.058

TABLE SII: High-symmetry points in the first Brillouin zone of the β and α phase. Coordinates are calculated by $\vec{k} = B_1\vec{b}_1 + B_2\vec{b}_2 + B_3\vec{b}_3$, in which \vec{b}_1 , \vec{b}_2 , and \vec{b}_3 are the reciprocal lattice vector. \vec{b}_1 , \vec{b}_2 , and \vec{b}_3 can be calculated by $(\vec{b}_1 \ \vec{b}_2 \ \vec{b}_3) = ((\vec{a}_1 \ \vec{a}_2 \ \vec{a}_3)^{-1})^T$

β phase				α phase			
	B_1	B_2	B_3		B_1	B_2	B_3
Γ	0.0000	0.0000	0.0000	Γ	0.0000	0.0000	0.0000
C	0.2662	0.2662	0.0000	T	0.5000	0.5000	0.5000
C_2	-0.2662	0.7338	0.0000	H_2	0.7641	0.2358	0.5000
Y_2	-0.5000	0.5000	0.0000	H_0	0.5000	-0.2358	0.2358
M_2	-0.5000	0.5000	0.5000	L	0.5000	0.0000	0.0000
D	-0.2580	0.7419	0.5000	S_0	0.3679	-0.3679	0.0000
D_2	0.2580	0.2580	0.0000	S_2	0.6320	0.0000	0.3679
A	0.0000	0.0000	0.5000	F	0.5000	0.0000	0.5000
L_2	0.0000	0.5000	0.5000				
V_2	0.0000	0.5000	0.0000				

TABLE III: Tight-binding parameters of β - Ga_2O_3 . \vec{R} is written in integer multiples of lattice vectors $[ijk]$ and can be translated to Cartesian coordinates by $\vec{R} = i\vec{a}_1 + j\vec{a}_2 + k\vec{a}_3$, where a_1 , a_2 , and a_3 are the lattice vectors.

onsite energy					hopping parameters continued				
site i	ϵ_i (eV)				site i	site j	\vec{R}	\tilde{t}_{ij} (eV)	ϕ_{ij}
Ga1, Ga2	4.95				Ga3 s	O1 px	[0,0,0]	0.355	0
Ga3, Ga4	4.52				Ga3 s	O1 px	[1,1,0]	0.355	0
all O	0				Ga3 s	O1 py	[0,0,0]	2.484	π
hopping parameters					Ga3 s	O1 py	[1,1,0]	2.484	0
site i	site j	\vec{R}	\tilde{t}_{ij} (eV)	ϕ_{ij}	Ga3 s	O1 pz	[0,0,0]	1.654	π
Ga1 s	Ga1 s	[1,1,0]	0.224	π	Ga3 s	O1 pz	[1,1,0]	1.654	π
Ga2 s	Ga2 s	[1,1,0]	0.224	π	Ga3 s	O3 py	[0,0,0]	2.162	π
Ga3 s	Ga3 s	[1,1,0]	0.129	0	Ga3 s	O3 py	[1,1,0]	2.162	0
Ga3 s	Ga4 s	[0,0,0]	0.108	0	Ga3 s	O3 pz	[0,0,0]	1.673	0
Ga3 s	Ga4 s	[1,1,0]	0.108	0	Ga3 s	O3 pz	[1,1,0]	1.673	0
Ga4 s	Ga4 s	[1,1,0]	0.129	0	Ga3 s	O4 px	[0,0,0]	2.878	0
Ga1 s	O1 px	[0,0,1]	0.652	0	Ga3 s	O4 pz	[0,0,0]	1.102	0
Ga1 s	O1 pz	[0,0,1]	3.467	0	Ga3 s	O5 px	[0,1,0]	2.965	π
Ga1 s	O3 px	[0,0,0]	2.592	0	Ga3 s	O5 pz	[0,1,0]	0.622	π
Ga1 s	O3 pz	[0,0,0]	2.592	π	Ga4 s	O2 px	[0,0,0]	0.352	π
Ga1 s	O6 px	[0,0,0]	1.748	π	Ga4 s	O2 px	[-1,-1,0]	0.352	π
Ga1 s	O6 px	[-1,-1,0]	1.748	π	Ga4 s	O2 py	[0,0,0]	2.484	0
Ga1 s	O6 py	[0,0,0]	3.029	0	Ga4 s	O2 py	[-1,-1,0]	2.484	π
Ga1 s	O6 py	[-1,-1,0]	3.029	π	Ga4 s	O2 pz	[0,0,0]	1.657	0
Ga1 s	O6 pz	[0,0,0]	0.440	π	Ga4 s	O2 pz	[-1,-1,0]	1.657	0
Ga1 s	O6 pz	[-1,-1,0]	0.440	π	Ga4 s	O3 px	[0,0,0]	2.878	π
Ga2 s	O2 px	[0,0,-1]	0.652	π	Ga4 s	O3 pz	[0,0,0]	1.102	π
Ga2 s	O2 pz	[0,0,-1]	3.467	π	Ga4 s	O4 py	[0,0,0]	2.164	0
Ga2 s	O4 px	[0,0,0]	2.596	π	Ga4 s	O4 py	[-1,-1,0]	2.164	π
Ga2 s	O4 pz	[0,0,0]	2.596	0	Ga4 s	O4 pz	[0,0,0]	1.663	π
Ga2 s	O5 px	[0,0,0]	1.750	0	Ga4 s	O4 pz	[-1,-1,0]	1.663	π
Ga2 s	O5 px	[1,1,0]	1.750	0	Ga4 s	O6 px	[0,-1,0]	2.965	0
Ga2 s	O5 py	[0,0,0]	3.030	π	Ga4 s	O6 pz	[0,-1,0]	0.622	0
Ga2 s	O5 py	[1,1,0]	3.030	0					
Ga2 s	O5 pz	[0,0,0]	0.443	0					
Ga2 s	O5 pz	[1,1,0]	0.443	0					

TABLE SIV: Tight-binding parameters of α - Ga_2O_3 . \vec{R} is written in integer multiples of lattice vectors $[ijk]$ and can be translated to Cartesian coordinates by $\vec{R} = i\vec{a}_1 + j\vec{a}_2 + k\vec{a}_3$, where a_1 , a_2 , and a_3 are the lattice vectors.

onsite energy				
site i			ε_i (eV)	
all Ga			-5.48	
all O			-10.5	
hopping parameters				
site i	site j	\vec{R}	\tilde{t}_{ij}	ϕ_{ij}
Ga1 s	Ga3 s	[0,0,0]	0.012	0
Ga1 s	Ga3 s	[-1,1,0]	0.013	0
Ga1 s	Ga3 s	[-1,0,1]	0.013	0
Ga1 s	Ga4 s	[0,0,1]	0.014	π
Ga1 s	Ga4 s	[0,-1,1]	0.010	π
Ga1 s	Ga4 s	[-1,0,1]	0.010	π
Ga2 s	Ga3 s	[0,0,0]	0.010	π
Ga2 s	Ga3 s	[0,1,0]	0.014	π
Ga2 s	Ga3 s	[-1,1,0]	0.010	π
Ga2 s	Ga4 s	[0,0,1]	0.013	0
Ga2 s	Ga4 s	[0,1,0]	0.013	0
Ga2 s	Ga4 s	[1,0,0]	0.013	0
Ga1 s	O1 px	[0,0,0]	1.983	0
Ga1 s	O1 py	[0,0,0]	0.105	0
Ga1 s	O1 pz	[0,0,0]	1.860	0
Ga1 s	O2 px	[-1,0,1]	0.910	π
Ga1 s	O2 py	[-1,0,1]	1.766	π
Ga1 s	O2 pz	[-1,0,1]	1.864	0
Ga1 s	O3 px	[0,0,0]	1.076	π
Ga1 s	O3 py	[0,0,0]	1.673	0
Ga1 s	O3 pz	[0,0,0]	1.867	0
Ga1 s	O4 px	[-1,0,1]	1.151	0
Ga1 s	O4 py	[-1,0,1]	2.402	π
Ga1 s	O4 pz	[-1,0,1]	1.248	π
Ga1 s	O5 px	[-1,1,0]	2.654	π
Ga1 s	O5 py	[-1,1,0]	0.216	0
Ga1 s	O5 pz	[-1,1,0]	1.246	π
Ga1 s	O6 px	[0,0,0]	1.509	0
Ga1 s	O6 py	[0,0,0]	2.197	0
Ga1 s	O6 pz	[0,0,0]	1.242	π
Ga2 s	O1 px	[0,1,-1]	1.511	π
Ga2 s	O1 py	[0,1,-1]	2.198	0
Ga2 s	O1 pz	[0,1,-1]	1.249	π
Ga2 s	O2 px	[0,0,0]	2.656	0
Ga2 s	O2 py	[0,0,0]	0.216	0
Ga2 s	O2 pz	[0,0,0]	1.242	π
Ga2 s	O3 px	[0,0,0]	1.142	π
Ga2 s	O3 py	[0,0,0]	2.404	π
Ga2 s	O3 pz	[0,0,0]	1.245	π
Ga2 s	O4 px	[0,1,0]	1.074	0
Ga2 s	O4 py	[0,1,0]	1.664	0
Ga2 s	O4 pz	[0,1,0]	1.866	0
Ga2 s	O5 px	[0,1,0]	0.904	0
Ga2 s	O5 py	[0,1,0]	1.759	π
Ga2 s	O5 pz	[0,1,0]	1.872	0
Ga2 s	O6 px	[0,1,0]	1.980	π
Ga2 s	O6 py	[0,1,0]	0.096	0
Ga2 s	O6 pz	[0,1,0]	1.870	0

hopping parameters continued				
site i	site j	\vec{R}	\tilde{t}_{ij} (eV)	ϕ_{ij}
Ga3 s	O1 px	[0,0,0]	1.508	π
Ga3 s	O1 py	[0,0,0]	2.191	π
Ga3 s	O1 pz	[0,0,0]	1.252	0
Ga3 s	O2 px	[0,0,0]	1.151	π
Ga3 s	O2 py	[0,0,0]	2.402	0
Ga3 s	O2 pz	[0,0,0]	1.251	0
Ga3 s	O3 px	[1,-1,0]	2.656	0
Ga3 s	O3 py	[1,-1,0]	0.199	π
Ga3 s	O3 pz	[1,-1,0]	1.253	0
Ga3 s	O4 px	[0,0,0]	0.910	0
Ga3 s	O4 py	[0,0,0]	1.779	0
Ga3 s	O4 pz	[0,0,0]	1.851	π
Ga3 s	O5 px	[0,0,0]	1.084	0
Ga3 s	O5 py	[0,0,0]	1.681	π
Ga3 s	O5 pz	[0,0,0]	1.853	π
Ga3 s	O6 px	[0,0,0]	1.995	π
Ga3 s	O6 py	[0,0,0]	0.098	π
Ga3 s	O6 pz	[0,0,0]	1.856	π
Ga4 s	O1 px	[0,0,-1]	1.989	0
Ga4 s	O1 py	[0,0,-1]	0.098	π
Ga4 s	O1 pz	[0,0,-1]	1.859	π
Ga4 s	O2 px	[-1,0,0]	1.077	π
Ga4 s	O2 py	[-1,0,0]	1.677	π
Ga4 s	O2 pz	[-1,0,0]	1.862	π
Ga4 s	O3 px	[0,0,-1]	0.908	π
Ga4 s	O3 py	[0,0,-1]	1.775	0
Ga4 s	O3 pz	[0,0,-1]	1.856	π
Ga4 s	O4 px	[-1,1,0]	2.653	π
Ga4 s	O4 py	[-1,1,0]	0.213	π
Ga4 s	O4 pz	[-1,1,0]	1.253	0
Ga4 s	O5 px	[0,1,-1]	1.151	0
Ga4 s	O5 py	[0,1,-1]	2.405	0
Ga4 s	O5 pz	[0,1,-1]	1.249	0
Ga4 s	O6 px	[0,0,0]	1.510	0
Ga4 s	O6 py	[0,0,0]	2.196	π
Ga4 s	O6 pz	[0,0,0]	1.254	0

TABLE SV: Tight-binding parameters of α - Al_2O_3 . \vec{R} is written in integer multiples of lattice vectors $[ijk]$ and can be translated to Cartesian coordinates by $\vec{R} = i\vec{a}_1 + j\vec{a}_2 + k\vec{a}_3$, where a_1 , a_2 , and a_3 are the lattice vectors.

onsite energy (eV)					hopping parameters continued				
site i	site j	\vec{R}	\tilde{t}_{ij}	ϕ_{ij}	site i	site j	\vec{R}	\tilde{t}_{ij} (eV)	ϕ_{ij}
all Al			7.00		Al3 s	O1 px	[0,1,-1]	0.924	0
all O			0.00		Al3 s	O1 py	[0,1,-1]	2.264	0
hopping parameters					Al3 s	O1 pz	[0,1,-1]	1.620	0
Al1 s	Al2 s	[0,-1,0]	1.019	π	Al3 s	O2 px	[-1,0,0]	1.644	π
Al1 s	Al3 s	[0,0,0]	0.429	0	Al3 s	O2 py	[-1,0,0]	2.699	π
Al1 s	Al3 s	[0,0,1]	0.389	0	Al3 s	O2 pz	[-1,0,0]	2.806	π
Al1 s	Al3 s	[1,0,0]	0.405	0	Al3 s	O3 px	[-1,1,0]	2.385	π
Al2 s	Al4 s	[0,0,0]	0.406	0	Al3 s	O3 py	[-1,1,0]	0.189	π
Al2 s	Al4 s	[1,0,0]	0.415	0	Al3 s	O3 pz	[-1,1,0]	1.636	0
Al3 s	Al4 s	[0,0,-1]	1.024	π	Al3 s	O4 px	[0,0,0]	1.476	0
Al1 s	O1 px	[0,0,0]	1.592	0	Al3 s	O4 py	[0,0,0]	2.108	π
Al1 s	O1 py	[0,0,0]	2.614	π	Al3 s	O4 pz	[0,0,0]	1.798	0
Al1 s	O1 pz	[0,0,0]	2.646	π	Al3 s	O5 px	[0,0,-1]	3.176	0
Al1 s	O2 px	[0,0,0]	1.008	π	Al3 s	O5 py	[0,0,-1]	2.857	π
Al1 s	O2 py	[0,0,0]	2.321	0	Al3 s	O6 px	[0,0,-1]	1.451	π
Al1 s	O2 pz	[0,0,0]	1.738	0	Al3 s	O6 py	[0,0,-1]	2.631	0
Al1 s	O3 px	[0,0,0]	1.553	0	Al3 s	O6 pz	[0,0,-1]	2.596	π
Al1 s	O3 py	[0,0,0]	2.708	0	Al4 s	O1 px	[-1,1,0]	2.510	π
Al1 s	O3 pz	[0,0,0]	2.685	π	Al4 s	O1 py	[-1,1,0]	0.197	0
Al1 s	O4 px	[0,0,0]	3.249	π	Al4 s	O1 pz	[-1,1,0]	1.727	π
Al1 s	O4 pz	[0,0,0]	2.871	π	Al4 s	O2 px	[-1,0,1]	1.468	π
Al1 s	O5 px	[0,0,0]	1.392	π	Al4 s	O2 py	[-1,0,1]	2.660	π
Al1 s	O5 py	[0,0,0]	2.058	π	Al4 s	O2 pz	[-1,0,1]	2.715	0
Al1 s	O5 pz	[0,0,0]	1.717	0	Al4 s	O3 px	[-1,0,1]	0.974	0
Al1 s	O6 px	[1,-1,0]	2.352	0	Al4 s	O3 py	[-1,0,1]	2.175	π
Al1 s	O6 py	[1,-1,0]	0.250	π	Al4 s	O3 pz	[-1,0,1]	1.606	π
Al1 s	O6 pz	[1,-1,0]	1.597	0	Al4 s	O4 px	[0,0,0]	1.535	0
Al2 s	O1 px	[0,1,0]	1.578	0	Al4 s	O4 py	[0,0,0]	2.022	0
Al2 s	O1 py	[0,1,0]	2.783	π	Al4 s	O4 pz	[0,0,0]	1.687	π
Al2 s	O1 pz	[0,1,0]	2.994	0	Al4 s	O5 px	[0,0,0]	3.038	0
Al2 s	O2 px	[0,0,0]	2.511	0	Al4 s	O5 py	[0,0,0]	2.702	0
Al2 s	O2 py	[0,0,0]	0.365	0	Al4 s	O6 px	[0,0,0]	1.619	π
Al2 s	O2 pz	[0,0,0]	1.704	π	Al4 s	O6 py	[0,0,0]	2.746	0
Al2 s	O3 px	[0,1,0]	1.473	0	Al4 s	O6 pz	[0,0,0]	2.903	0
Al2 s	O3 py	[0,1,0]	2.567	0					
Al2 s	O3 pz	[0,1,0]	2.657	0					
Al2 s	O4 px	[0,1,0]	2.998	π					
Al2 s	O4 pz	[0,1,0]	2.722	0					
Al2 s	O5 px	[0,1,-1]	1.381	π					
Al2 s	O5 py	[0,1,-1]	1.901	0					
Al2 s	O5 pz	[0,1,-1]	1.554	π					
Al2 s	O6 px	[0,0,0]	1.144	π					
Al2 s	O6 py	[0,0,0]	2.297	π					
Al2 s	O6 pz	[0,0,0]	1.769	π					